A phase width for CaGaSn. Crystal structure of mixed intermetallic Ca4Ga4+xSn4–x and SmGaxSn3–x, stability, geometry and electronic structure

Monique Tillard

A phase width for CaGaSn. Crystal structure of mixed intermetallic $Ca_4Ga_{4+x}Sn_{4-x}$ and $SmGa_xSn_{3-x}$, stability, geometry and electronic structure.

Monique TILLARD

Institut Charles Gerhardt Montpellier, Département CSMD équipe AIME
UMR 5253 CNRS-UM-ENSCM, CC1502
Université de Montpellier
2 Place Eugène Bataillon
34095 Montpellier cedex 5 – France

Email : mtillard@univ-montp2.fr, phone 33 4 67 14 48 97, fax 33 4 67 14 33 04.

Abstract

X-ray single-crystal structure has been established for new compositions in intermetallic systems of tin and gallium. Crystals were successfully obtained in alloys prepared from elements. The structure of $SmGaSn_2$ (cubic $Pm\overline{3}m$, a = 4.5778(8) Å, Z = 1, R1 = 0.012) is described with atomic disorder at all Sn/Ga positions and the structure of $Ca_4Ga_{4.9}Sn_{3.1}$ (hexagonal, $P6_3/mmc$, a = 4.2233(9), c = 17.601(7) Å, Z = 1, R1 = 0.062) raises an interesting question about existence of a composition domain for CaGaSn. Finally, $Ca_4Ga_{4.9}Sn_{3.1}$ should be considered as a particular composition of $Ca_4Ga_{4+x}Sn_{4-x}$, a compound assumed to exist in the range x ~ 0 - 1. Partial atomic ordering characterizes the Sn/Ga puckered layers of hexagons whose geometries are analyzed and discussed comparatively with analogous arrangements in AlB_2 related hexagonal compounds. The study is supported by rigid band model and DFT calculations performed for different experimental and hypothetic arrangements.

Keywords: Intermetallic compounds; Tin; Gallium; Crystal structure; DFT calculations

1. Introduction

Numerous ternary combinations that involve tin and gallium are known and structurally characterized. Among the reports listed in the Pearson crystal database, a great number of compositions mainly includes Ba and adopts the famous clathrate type structures. In these ternary compounds, Sn and Ga atoms are 4-bonded within tridimensional networks composed by large cages that enclose Ba atoms. These arrangements are affected by some atomic disorder since Sn and Ga at cage vertices are statistically mixed at metal atoms positions. Various structures are described for the remaining compounds that contain p-block or transition elements. The M^V–Sn–Ga compounds have been subject of interest for their superconducting behavior [1], [2], [3], [4] and [5] and the Sn/Ga atom distribution in structures would play a role in their properties. Combinations that involve electropositive elements display more or less complicated intermetallic frameworks, as for example, layers in SrGaSn [6], double layers in Li_5Ga_4 [7], infinite chains of clusters in $Na_{10}Ga_6Sn_3$ [8] or complex 3D network in $Na_3Ga_8Sn_3$ in which coexist clusters and waved layers [9]. In most cases, Sn and Ga atoms are 4-bonded within networks and Sn/Ga atom disorder is often reported.

Only two compounds with very simple stoichiometries contrast with this general trend, SrGaSn and CaGaSn [6]. The structure of SrGaSn is described without atomic mixing and was solved from single-crystal diffraction while CaGaSn was stated isostructural on the basis of its similar powder pattern. Their hexagonal structure is related to the AlB_2 structure-type in which alkaline-earth atoms occupy Al positions while Sn and Ga alternately fill the boron sites. Each metal atom on the hexagon network is then linked to three neighbors different in nature, it results in a waving of the layers which remain without any bonding interactions, as attested by shortest interlayer distances of 3.30 and 3.98 Å at Ga-Ga pairs in SrGaSn and CaGaSn, respectively.

These structures fairly remind those of Li_3Ga_2 [10] and Li_5Ga_4 [7] Zintl compounds also deriving from the AlB_2 structure. Layers therein are puckered and composed of 3-bonded Ga atoms (partially reduced by Li) at two independent crystallographic sites. Beyond the atom nature, the structural arrangements in Li_3Ga_2 and Li_5Ga_4 differ from that in SrGaSn by the staggered position of consecutive layers. Since layers are shifted against each other, interlinking is prevented in Li_3Ga_2. Instead, the shift two-by-two of the layers in Li_5Ga_4 allows association into double layers through Ga-Ga bonding of 2.68 Å.

The present work reports on two ternary intermetallic compounds of tin and gallium for which single crystal structures are determined. The compound $SmGaSn_2$ displays an original network for a ternary composition and the hexagonal structure of $Ca_4Ga_{4.9}Sn_{3.1}$ raises questions about the existence of a phase width for CaGaSn. Structural descriptions, network and bonding analyses are supported by DFT calculations.

2. Experimental section

The elements Ga (Rhone Poulenc, 6N), lumps of Sn and Sm (Alfa Aesar, 99.9%), Ca (Merck, 99%) were taken without further purification. Stoichiometric amounts were weighed to prepare alloys at compositions $SmGa_3Sn_2$ and $Ca_5Ga_9Sn_4$, they were inserted in Ta tubes weld-sealed under argon atmosphere and protected from oxidation in Ar-filled sealed stainless steel jackets. Samples were heated to 900 °C for 16 h in a classical tubular furnace and then submitted to slow cooling at 10 °/h. The well crystallized products were handled under argon atmosphere, several crystals could be selected using a microscope placed in the glove box and then sealed into capillaries to be checked for crystallinity. The best diffracting single crystals that display the required quality were used for X-ray diffraction data collection and were further analyzed to establish their composition. EDX

measurements were performed using an Oxford Instrument Environmental Scanning Electron Microscope, equipped with an X-Max large area SDD sensor that allows excellent sensitivity/precision/resolution. The EDX analysis led to Sm:Ga:Sn and Ca:Ga:Sn ratios of 26.4:24.1:49.5 and 33.5:37.9:29.1, respectively. Crystal structures were solved [11] and refined [12] using SHELX programs. Details on single crystal data collection and structural refinements are given in table 1. Atom disorder Sn/Ga was considered for the two compounds and site occupation factors were refined together with atom positions and anisotropic displacement parameters. Within the standard deviation limits, site occupation at all positions does not deviate from full site occupancy. The final refined compositions from X-ray study are $SmGaSn_2$ and $Ca_4Ga_{4.9}Sn_{3.1}$, respectively. They quite well agree with atom proportions found from the EDX analysis of the single crystals previously used for diffracted intensity recording. It is noteworthy that Ga content is fairly lower in compounds than in the prepared alloys, this may underline the role of a Ga excess in the crystallization processes. The final refined atom positions and equivalent displacement parameters are given in Table 2. Further details on crystal structures may be obtained from FIZ Karlsruhe (crysdata@fiz-karlsruhe.de) on quoting the CSD deposition numbers 431519 ($Ca_4Ga_{4.9}Sn_{3.1}$) and 431520 ($SmGaSn_2$).

3. Calculation Method

Calculations at the DFT level have been performed with the code CASTEP [13] using the gradient-corrected GGA-PW91 exchange and correlation functional [14]. CASTEP uses plane-wave basis sets to treat valence electrons and pseudo potentials to approximate the potential field of ion cores. Ultra-soft pseudo potentials (USPP) generated for each element according to the Vanderbilt [15] scheme were chosen. Tin was taken with four $5s^2\ 5p^2$ valence states and calcium with ten $3s^2\ 3p^6$

$4s^2$ valence states. The inner 3*d* and 4*f* levels were respectively considered for Ga $3d^{10}$ $4s^2$ $4p^1$ and Sm $4f^6$ $5s^2$ $5p^6$ $6s^2$. Kinetic cut-off energies were set at ultrafine qualities (330 and 420 eV) and a Monkhorst-Pack grid of automatically generated *k*-points was used for numerical integration in the Brillouin zone [16].

All along this work, both atom positions and unit cell dimensions were fully relaxed in the geometry optimizations performed at the DFT level by minimizing the total energy. Calculations were carried out within the experimental cubic $Pm\bar{3}m$ symmetry for Sm compounds, instead the P3m1 symmetry (which is common to all arrangements) was used for the hexagonal models in cells containing four layers.

Density of states DOS and crystal overlap populations COOP have also been calculated for CaGaSn using a rigid band model within the tight binding extended Hückel method provided in CAESAR2 package [17].

4. Results and Discussion

The structural representation of compounds $SmGaSn_2$ and $Ca_4Ga_{4.9}Sn_{3.1}$ given in figure 1 highlights the differences in p-block sub-lattices yet characterized with a common feature, namely the occurrence of Sn/Ga atomic mixing.

4.1. $SmGaSn_2$ structure

Compound $SmGaSn_2$ crystallizes within cubic $Pm\bar{3}m$ symmetry with a = 4.5778(8) Å. Its structure is easily visualized as a 3D network of octahedral units sharing all vertices. Sn and Ga are statistically mixed on octahedra at the unique *3c* (0,½,½) position and separated by 3.267 Å (octahedra edges) from alike neighbors. At origin of the cell, Sm atom is located at the center of a

cuboctahedron formed by 12 Sn/Ga atoms. The Sn to Ga atomic proportion, freely refined in the structural refinement, converges to 2 and then the compound can be formulated $Sm[GaSn_2]$. Its structure belongs to the $AuCu_3$-type and is so far not observed for ternary tin and gallium combinations. Some isostructural ternary compounds including Sn have been already reported with atom mixing in their structure but it involves only the electropositive atom positions [18].

Table 1. Crystal data and structure refinement

Compound	**$SmGaSn_2$**	**$Ca_4Ga_{4.9}Sn_{3.1}$**
Initial composition (alloy)	$SmGa_3Sn_2$	$Ca_5Ga_9Sn_4$
Refined composition	$SmGa_3Sn_{2.00(1)}$	$Ca_4Ga_{4.91(3)}Sn_{3.09(3)}$
Crystal system	cubic	hexagonal
Space group	$Pm\overline{3}m$	$P6_3/mmc$
Lattice parameters (Å)	4.5778(8)	4.4233(9), 17.601(7)
Volume ($Å^3$)	95.93(5)	298.24(17)
Crystal size (mm)	0.05×0.06×0.10	0.05×0.10×0.10
F(000)	193	387
Absorption coefficient (mm^{-1})	34.63	18.9
θ range (deg)	4.45-45.35	2.31-29.88
Diffractometer	Oxford Xcalibur CCD	Nonius CAD4
Extinction coefficient ($\times 10^{-4}$)	0.011(1)	
Independent reflections	114 [R(int) = 0.0470]	204 [R(int) = 0.0475]
Goodness-of-fit on F^2	1.074	1.191
Final R1/wR2 indices [$I > 2\sigma(I)$]	0.0084/0.0207	0.0418/0.1042
R1/wR2 indices (all data)	0.0118/0.0212	0.0673/0.1142
Residual densities (e. $Å^{-3}$)	0.95/-0.74	3.60/-2.46

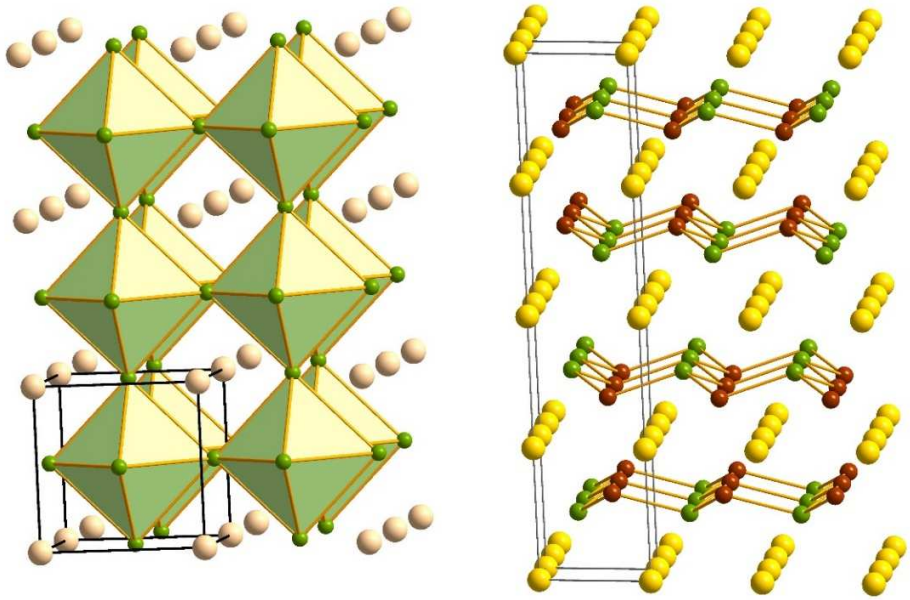

Figure 1: Representation of cubic $SmGaSn_2$ and hexagonal $Ca_4Ga_{4.9}Sn_{3.1}$ structures.

This structural type is also adopted by $SmSn_3$ and $NpSn_3$, two binary compounds known as intermetallic heavy fermions whose interest is to display superconducting behavior at low temperature [19]. Note also that no structure has been reported in the literature for $SmGa_3$, a stoichiometry yet included in the composition domain of ε-$SmGa_x$ ($2 < x < 4$) with structures reminiscent of AlB_2 type [20] and [21]. Even simply regarded as derived from $SmSn_3$ by atomic substitution, compound $SmGaSn_2$ deserves some attention since incorporation of gallium and occurrence of atom disorder in its structure may affect the physical properties. Replacement of Sn by Ga occurs at the unique crystallographic site *3c* which is statistically occupied by one third of Ga atoms within the cubic symmetry (no additional diffraction spots). This atom substitution is responsible for the 6.5% contraction of the lattice volume compared to experimental $SmSn_3$. Geometries optimized at the DFT level (conditions described above) are in agreement with this lattice contraction and confirm that the cubic symmetry is retained for both $SmSn_3$ and the ordered

$SmGaSn_2$ models. The density of states calculated for $SmSn_3$ and for $SmGaSn_2$ are very similar, particularly displaying a peak intensity at Fermi level.

Table 2. Positional and atomic equivalent displacement parameters. U_{eq} is defined as one third of the trace of orthogonalized U_{ij} tensor.

$SmGaSn_2$

	Position	occupation	x	y	z	U_{eq} (Å^2)
Ga	*3c*	0.334(4)	0	1/2	1/2	0.0180(1)
Sn		0.666(4)				
Sm	*1a*	1	0	0	0	0.01296(7)

$Ca_4Ga_{4.9}Sn_{3.1}$

		Position	occupation	x	y	z	U_{eq} (Å^2)
M1	Sn	*4f*	0.773(2)	1/3	2/3	0.38497(6)	0.0077(4)
	Ga		0.227(2)				
M2	Ga	*4f*	1	2/3	1/3	0.3414(2)	0.0250(7)
Ca1		*2a*	1	0	0	0	0.0135(9)
Ca2		*2b*	1	0	0	0.25	0.0146(9)

4.2. $Ca_4Ga_{4.9}Sn_{3.1}$ structure

The unit cell of $Ca_4Ga_{4.9}Sn_{3.1}$ with dimensions a = 4.2233(9) and c = 17.601(7) Å displays the hexagonal $P6_3/mmc$ symmetry and belongs to the YPtAs-type as do the isostructural CaGaSn (a = 4.44, c = 17.53 Å [6]) and SrGaSn (a = 4.55, c = 18.71 Å) [6] and [22]. These structures derive from the hexagonal P6/mmm structure of AlB_2 with Ca or Sr lying at the Al positions in interlayer space while Sn and Ga share the boron sites on hexagon layers. Subsequently layers in these ternary compounds are heteroatomic and no longer planar, thus the structural type YPtAs may be viewed

as a superstructure of AlB_2 by atomic differentiation and hexagon tilting. In the structure of $Ca_4Ga_{4.9}Sn_{3.1}$, Ca fills *2a* and *2b* sites while heavier Sn and Ga are located at two cristallographically independent *4f* positions. During the structural refinement, mixing of Sn and Ga atoms was considered at these *4f* sites but it rapidly appeared that the substitution of Sn for Ga preferentially occurs at M1 site. At this position, the proportion of Sn reaches ~80 % while it remains close to zero at M2. This leads to a refined composition $Ca_4Ga_{4.7}Sn_{3.3}$ which is fairly close to $Ca_4Ga_{4.5}Sn_{3.5}$, the composition established by analysis for the studied single crystal. However, according to standard deviations, the very low Sn content at M2, refining to 0.001(6), must be regarded as zero. Therefore, the final refinement has been performed with the M2 site entirely filled with Ga, leading to the slightly changed formulation $Ca_4Ga_{4.9}Sn_{3.1}$, therefore used for the compound.

4.3. Layer packing in hexagonal structures

Before further analyzing the structural and geometrical parameters, let us have a look at the hexagon layers and their packing in various hexagonal structures. In the AlB_2 parent [23], boron atoms are arranged within graphite-like planar layers stacked on top of each other and the Al atoms in the interlayer space are directly placed below and above hexagon centers. Boron atoms therein are 3-bonded and involved in B–B bonds of 1.79 Å within the layer while no bonding interaction occurs between layers separated by 3.26 Å. Note that the layer separation is reduced to 3.08 Å in isostructural MgB_2 [24] known with special superconducting properties. Likewise, some ternary compounds are built with planar hexagon layers within the BaLiSi structure-type [25], as SrAlSi [26] or SrAlGe [27], or within the ZrBeSi structure-type [28], as LiBC [29]. One can note that superconductivity of some of these compounds, as for example CaAlSi and SrAlSi, has been investigated for their structural similarity with MgB_2 [30].

Instead, layers may also deviate from flatness and stack in various ways as for instance with the same orientation in $EuGe_2$ structure-type [31] or with opposite orientations in $CaIn_2$ structure-type [32] (figure 2).

A great number of ternary compounds are found to display puckered layers of hexagons. Nevertheless, the atomic composition, the ordering of atoms, the relative arrangement of layers and the level of distortion produce deviations to symmetry. Consequently the resulting structures belong to various space groups. A comprehensive study provides a description of structural relationships for structures originating from the AlB_2-type and underlines the various distortions being the expression of flexibility and variety of the chemical bonding in these superstructures [33]. Among compounds that adopt the YPtAs structural type, one can cite the LnZnSn family of intermetallic compounds characterized with an ordered atom arrangement and a quasi-constant Zn-Sn bond length within the layers [34] and [35] whilst the Zn-Zn interlayer separation gradually increase along the series. For the ordered YbGaGe compound, a tolerance of a certain compound deviation has been evidenced [36] and [37] leading to occurrence of atom mixing in layers. Also interesting is the effect of atomic nature on the tendency of hexagon networks to pucker. Thereby Si and Ga are randomly distributed in plans of hexagons in EuGaSi structure of AlB_2-type while Ga and Ge (or Sn) are arranged orderly in EuGaGe (or EuGaSn) structures of YPtAs-type [38]. Structures of $Eu(Ga_{1-x}T_x)_2$ compounds supply a beautiful example of structural evolution with the composition, from the orthorhombic KHg_2 to hexagonal AlB_2 and further to tetragonal $ThSi_2$ types, when T = Si. Instead for T = Ge, it changes step by step from KHg_2 for hexagonal YPtAs and finally for trigonal $EuGe_2$ via complex and disordered higher superstructures [39].

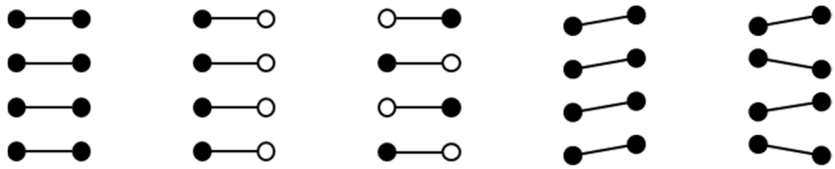

Figure 2: Schematic representation of the packing of hexagon layers in

left to right AlB_2 [23], BaLiSi [25], ZrBeSi [28], $EuGe_2$ [31] and $CaIn_2$ [32] structure-types

It is then convenient to define some useful parameters to compare the different structures and specially to quantify the geometry distortions. The flatness deviation of layers can be expressed by the angles α_n and the relative position of successive layers by the interlayer distances d_n (figure 3). In the AlB_2 parent structure, with planar equidistant layers, α_n angles are 120° and all d_n distances are equal to 3.26 Å. Starting from a planar sp^2 configuration with a 120° angle, the puckering of hexagon layers will reduce the value of the angle towards 109.45° which corresponds to the tetrahedral sp^3 configuration.

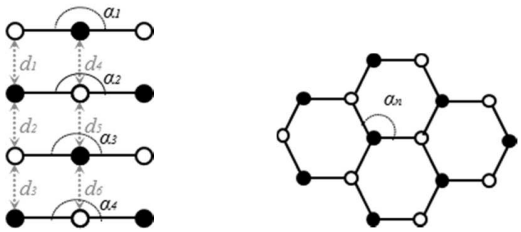

Figure 3: Typical parameters (angles and distances) to define the geometry of hexagon layers

Various kinds of stacking are encountered in binary or ternary structures containing layers, partly or entirely composed of gallium, that are not any more planar (figure 4). Structure of Li_3Ga_2 [10] can be derived from AlB_2 by folding the layers of 3-bonded Ga atoms (2.67 Å) and then by shifting

the layers relative to one another. Layers with same orientations are arranged so that the shortest Ga–Ga interlayer distance is 4.51 Å, with a thick and complex sheet of Li atoms in the interlayer space.

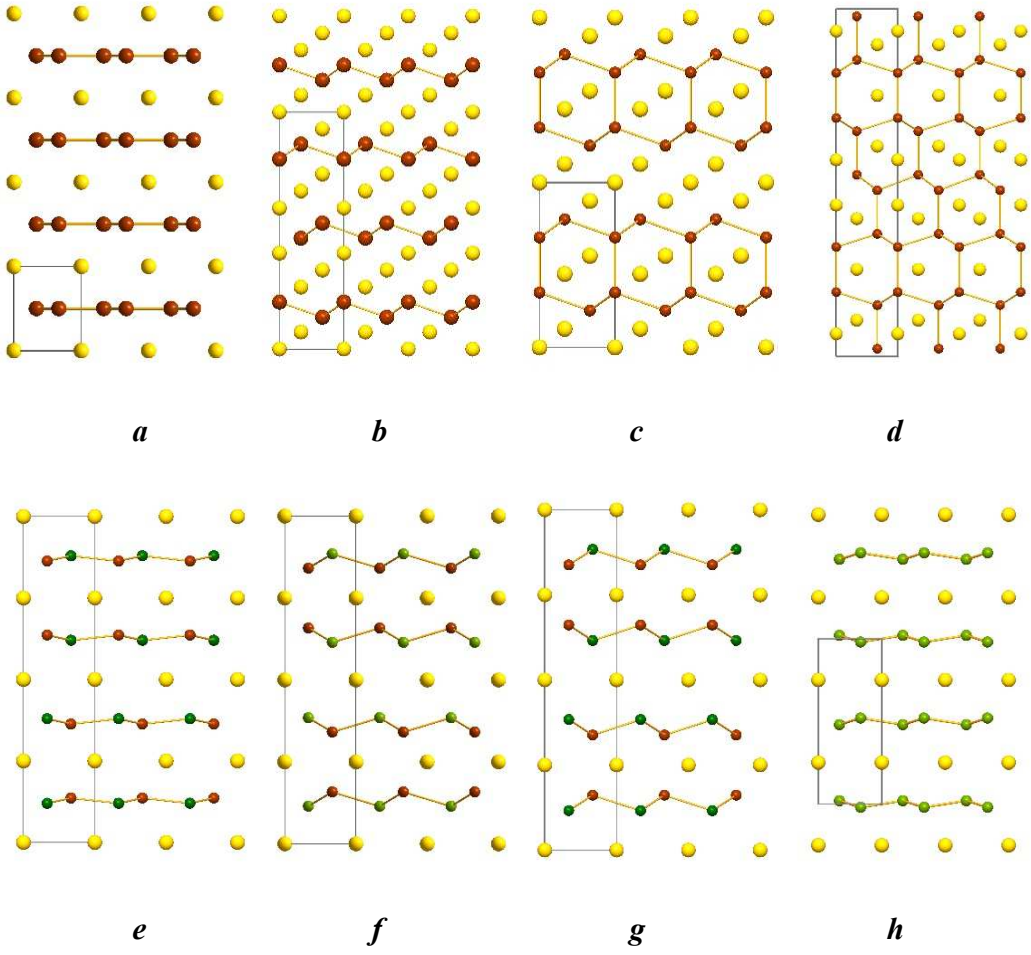

Figure 4: [100] structural projections showing the packing of hexagon layers in *a*- AlB_2 [23], *b*- Li_3Ga_2 [10], *c*- Li_5Ga_4 [7], *d*- Li_2Ga_2Sn [40], *e*- $Ca_4Ga_4Sn_4$ [6], *f*- $Ca_4Ga_{4.9}Sn_{3.1}$ [this work], *g*- $Sr_4Ga_4Sn_4$ [6], *h*- $Ba_4Ga_4Sn_4$ [22]. Unit cells limits are drawn as grey lines.

A more substantial shift occurs in Li_5Ga_4 [7] leading in two-by-two interconnection of the layers through Ga–Ga bonds of 2.78 Å, slightly longer than bonds within layers (2.68 Å). Note that the angles α are 109.5° in Li_3Ga_2 and 109.3° in Li_5Ga_4 and very close to the tetrahedral angle. A more thorough condensation of hexagon layers is achieved in the structure of ternary compound Li_2Ga_2Sn in which Sn and Ga are statistically disordered in 1:2 proportion or in other words mixed at all sites [40]. In this structure, a three dimensional network is built with bonds between layers (2.71 - 2.81 Å) that are just slightly longer than bonds within layers (2.67 - 2.72 Å). With α angles ranging from 108.2 to 111.2°, the mean deviation to flatness remains of the same order as in the previous binary compounds. Layers in these Ga-containing structures may be regarded as built with 3-bonded atoms involved in homoatomic connections. Actually, Ga–Ga bonding occurs in binary combinations, and M–M bonding occurs in Li_2Ga_2Sn within layers composed of M pseudo-atoms (Sn and Ga distributed in 1:2 proportion at all M sites). Note that additional bonding occurs between layers in Li_5Ga_4 and Li_2Ga_2Sn.

Things are somewhat different in $Ca_4Ga_4Sn_4$ (or CaGaSn) as in isostructural $Sr_4Ga_4Sn_4$ where Sn and Ga atoms are found with a totally ordered distribution, the layers being there characterized by true heteroatomic Sn–Ga bonding. Despite the presence of some atomic mixing in $Ca_4Ga_{4.9}Sn_{3.1}$, the repartition of atoms within the layers is so that only M–Ga bonds are formed that involve M pseudo atoms (Sn and Ga in 4:1 proportion) giving a heteroatomic character to bonding. The M–Ga bond length of 2.667 Å in $Ca_4Ga_{4.9}Sn_{3.1}$ is typical for covalently bonded atoms and must be compared with sum of covalent radii of the elements, respectively 2.52, 2.66 and 2.80 Å for Ga–Ga, Sn–Ga and Sn–Sn bonds. Even if the organization of layers in $Ca_4Ga_{4.9}Sn_{3.1}$ reminds that in Li_5Ga_4, the layers are too distant to allow interconnections. The shortest distance of 3.22 Å between layers occurs at Ga pairs and compares well with the alike distances of 3.30 or 3.35 Å, calculated for $Sr_4Ga_4Sn_4$ from the available data [6] and [22]. The small lengthening in $Sr_4Ga_4Sn_4$ could be

attributed to the increase in radius of the electropositive element (1.34 for Ca^{2+} and 1.44 for Sr^{2+} ionic radii [41]). Likewise, the value of α angle of 112.1° is very close to that reported for $Sr_4Ga_4Sn_4$ combination (111.1 or 111.6°). Noteworthy are these values of angle, higher than in Li combinations mentioned above, that indicate a weaker waving of the layers with the heavier electropositive elements.

It is important at this stage to point out the discrepancy in geometrical features for the two isostructural compositions of the Ca compound, however both consistent with the $Ca_4Ga_{4+x}Sn_{4-x}$ formula. Curiously a much larger distance of 3.98 Å is reported for $Ca_4Ga_4Sn_4$ [6] with also a very high angle of 118.8° meaning that layers are almost planar (only deviating by 1.2°). Seemingly, an increase by ~1 in the Ga-content (from $Ca_4Ga_4Sn_4$ to $Ca_4Ga_{4.9}Sn_{3.1}$) amplifies the waving of layers and reduces the distance between layers. At the same time, within layers, M−Ga bonds are elongated from 2.579 Å to 2.667 Å when Ga partially replaces Sn at M1 site. This does not appear really consistent with the covalent radii of the elements (1.26 Å for Ga and 1.40 Å for Sn) and might suggest a non-zero probability for the substitution of Ga for Sn at M2 site in $Ca_4Ga_{4.9}Sn_{3.1}$. Despite that, it is quite confusing to find larger differences in geometry between $Ca_4Ga_{4.9}Sn_{3.1}$ and $Ca_4Ga_4Sn_4$ differing by the layer content than between $Ca_4Ga_{4.9}Sn_{3.1}$ and $Sr_4Ga_4Sn_4$ contrasting by the nature of species in the interlayer space. These observations tend to indicate that size of the electropositive component would have a weak influence on the structural geometry, but comparison with the structure of BaGaSn does not confirm this statement. According to the literature, BaGaSn ($Ba_4Ga_4Sn_4$) is indeed described in the hexagonal $P6_3/mmc$ symmetry with weakly puckered layers (α = 117.7°) in which Sn and Ga are mixed in equal proportion at all positions [22] and [42]. Moreover, BaGaSn lattice is smaller, with a = 4.58, c = 10.33 Å and the orientation of layers does not agree with the YPtAs structure-type. At a first glance, one can imagine that a larger supercell might have been missed, but a detailed diffraction study

unambiguously established that BaGaSn should be considered as a ternary disordered compound, isostructural with $CaIn_2$ (figure 2).

Trying to understand these peculiarities, the geometry has been optimized for several ordered models (S1, D1, S3, D3 and D5, see in figure 5) built in a double cell that contains four layers. Lattices do not deviate by more than 2% from the experimental, and planar geometry is never retained for the layers. The lowest total energy is calculated for model D3 associated to YPtAs structure-type but it only differs by 0.02 and 0.09 eV from the energies computed for models S3 and D5 associated with $CaIn_2$ structure-type. One could then conclude that, only on an energetic point of view, an ordered $Ba_4Ga_4Sn_4$ arrangement can exist under several geometries, a result which is likely to be modified by atomic disorder at all sites.

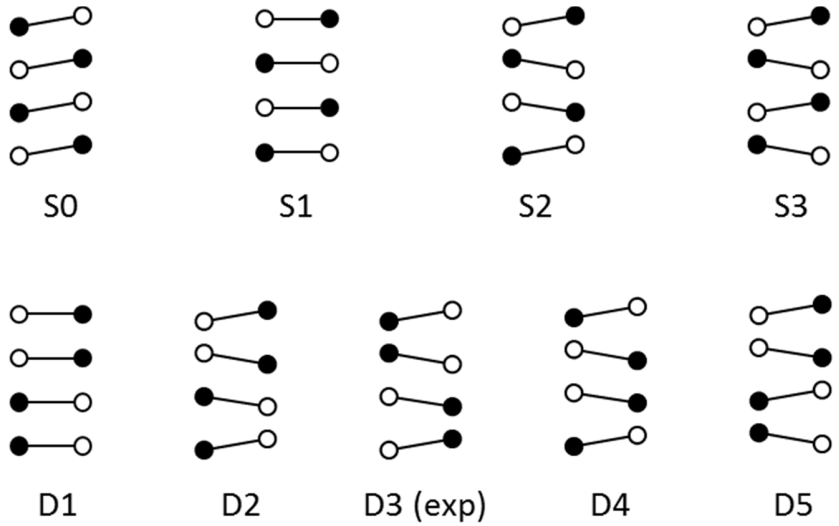

Figure 5: Packing modes within hexagonal lattices. The models are built with four layers of A-type (○—●) or B-type (●—○). The ABAB packing leads to S models while AABB packing gives D models. For clarity, the electropositive atoms are not represented.

4.4. A composition domain for $Ca_4Ga_4Sn_4$?

The characterization of a crystal whose composition $Ca_4Ga_{4.9}Sn_{3.1}$ deviates from the already known $Ca_4Ga_4Sn_4$ raises questions about coexistence in the ternary Ca-Sn-Ga system of two "line compounds" with close compositions and same structure. It is more reasonable to believe that these stoichiometries are included into a solid solution domain around CaGaSn, but the limits of such a domain remain unknown. Since no report was found on $CaSn_2$ structure, the domain should be a priori limited on the tin-side. On the other hand, the existence of $CaGa_2$ ($P6_3/mmc$, a = 4.4, c = 7.3 Å [43]) could let foresee an extension on the Ga-rich side. Nevertheless, in spite of its hexagonal structure, $CaGa_2$ cannot be seen like a substructure of such a compound because of differences in the orientation of layers, which corresponds either to S3 arrangement in $CaGa_2$ or to D3 arrangement in $Ca_4Ga_{4+x}Sn_{4-x}$ (figure 5). Within a solid solution domain, the lattice dimensions are expected to follow a Vegard's law, especially in case of a progressive substitution phenomenon. The c parameter of the hexagonal cell, directly related to the layer stacking, is then likely to vary significantly with the substitution. Remembering that substitution is only found at M1 site in $Ca_4Ga_{4.9}Sn_{3.1}$, it is plausible that the domain would be limited to $0 \leq x \leq 1$ for the $Ca_4Ga_{4+x}Sn_{4-x}$ formulation. To evaluate the probability for $CaGa_2$ to also exist within D3 configuration, its geometry was optimized starting from experimental S3 and hypothetical D3 models in 1×1×2 supercells. The total energy per $CaGa_2$ formula unit differs by 0.13 eV in favor of the experimental S3 configuration, this corroborates the assumption of a limited phase width around $Ca_4Ga_4Sn_4$.

4.5. Geometry and stability of $Ca_4Ga_{4+x}Sn_{4-x}$ models

Considering the many possibilities to stack hexagon layers which provide structures being different by the atom arrangement and the orientation of layers, a theoretical approach is likely to improve our understanding of $Ca_4Ga_{4+x}Sn_{4-x}$. The study attempts to establish the relative stabilities of

various models based on the experimental structure and to evaluate their dependence on composition. Models built from experimental lattice include four layers and correspond to one $Ca_4Ga_4Sn_4$ formula unit. The repeat unit contains four atom pairs of A-type (Ga–Sn) or B-type (Sn–Ga) packed along the hexagonal c-axis and four Ca atoms used in calculations but not drawn in the schematic representations given in figure 5.

Packing alternately the layers in ABAB mode leads to S models while AABB mode gives D models. Note that orientation of the layers is identical in models S2, D2, D4 and in the $Ca_4Ga_{4+x}Sn_{4-x}$ experimental D3 configuration. While the planar model S1 corresponds to ZrBeSi structure-type, the puckered model S3 agrees with NdPtSb structure-type [44]. Instead, models S0, D1 and D5 can be seen as ternary derivatives of $EuGe_2$, AlB_2 and $CaIn_2$, respectively (see in figure 2). Geometry has been optimized for nine models in the conditions described previously within the common P3m1 symmetry and in some cases additionally within the actual symmetry. The optimized lattice dimensions, the characteristic distances and angles are given together with total energies and formation enthalpies in supplementary material. The formation enthalpy which allows a good evaluation of the stability is defined as total energy of the compound minus total energies of the elements, calculated in their solid state structures.

The total energy and the formation enthalpy calculated for $Ca_4Ga_4Sn_4$ with various arrangements are given in Figure 6. It clearly appears that models D1 and D3 distinguish from all other configurations by their high negative values of enthalpy/energy, a sign of stability. One must remark that starting arrangement (*i.e.* layer orientation) is maintained for all the optimized except planar models. The planar model S1 (ABAB packing mode) evolves towards the S0 "in-phase" waving geometry and the model D1 (AABB packing mode) converts upon optimization to the D3 experimental geometry. Note that all the symmetry constrained calculations –$P6_3/mmc$, P3m1 and P1– for the D3 experimental arrangement led to optimized geometries that perfectly obey the

$P6_3/mmc$ symmetry as checked by using the "find symmetry" tool under the most strict (ultra-fine) tolerance conditions.

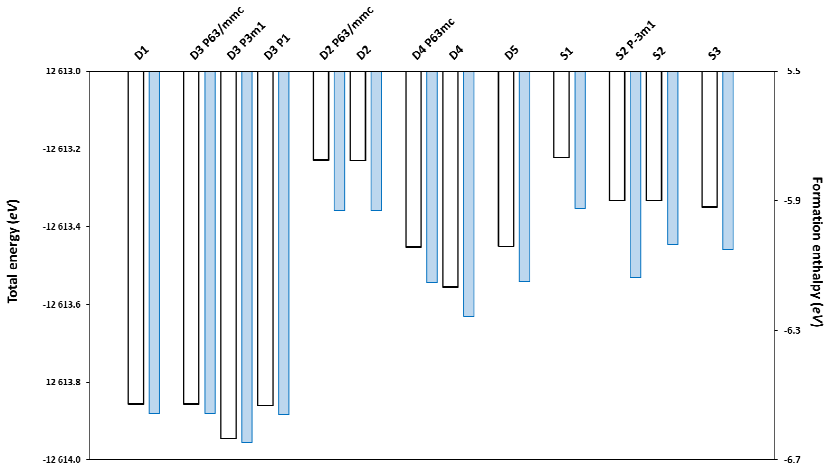

Figure 6: Total energy (empty bars) and formation enthalpy (filled bars) calculated for various arrangements within P3m1 (and other) symmetry constraints.

Calculation predicts an angle value close to 109° for this D3 geometry. The experimental angle of 118.82° measured in $Ca_4Ga_4Sn_4$ [6] is far for this expectation, even out of range of angles optimized in Ga–Sn layers, and is rather close to the angles optimized in pure gallium layers. Also strange is the disparity between experimental (3.979 Å) and optimized (2.979 Å) values of the shortest distances between layers in $Ca_4Ga_4Sn_4$. On the contrary, it should be remarked that a much better agreement is observed in the isostructural $Sr_4Ga_4Sn_4$, with optimized angle of 111.4° and distance of 3.303 Å in accordance with the experimental values of 111.0° and 3.30 Å [6] or 111.6° and 3.35 Å [22]. For $Ba_4Ga_4Sn_4$, the difference between the optimized ordered models S3 and D5 derived from $CaIn_2$ (114° and 4.5 Å) and the experimental structure (117.7° and 4.75 Å) could be explained by the totally disordered atomic distribution within the layers. Nevertheless, one observes angle

opening and layer flattening when the size of electropositive element is increased, just as in the MGa_2 series with layers that are puckered for Ca and nearly planar for Sr and Ba.

4.6. Atomic disorder effects

Thereafter, additional models were constructed by replacing at second layer one Ga by one Sn or vice versa. These new models correspond to $Ca_4Ga_3Sn_5$ and $Ca_4Ga_5Sn_3$ compositions and might be useful to evaluate the changes in geometry and in stability caused by the occurrence of Sn/Ga atomic disorder. Also the study of these Sn-rich and Ga-rich models should bring elements to validate and delimit the $Ca_4Ga_{4+x}Sn_{4-x}$ phase width. Except for planar models S1 and D1, the optimized geometries preserve initial arrangements and orientation of layers. As expected and whatever the model, the homoatomic layer implicated in atom substitution is strongly disturbed, the neighboring layers being affected at a very less extent. Let us recall that α angle varies in range 108-111° for Sn–Ga layers in $Ca_4Ga_4Sn_4$ optimized models. In Sn enriched models, the angle is significantly reduced to ~101° at the homoatomic layer which is strongly puckered. In contrast, the homoatomic layer is flattened in the Ga enriched models with angles comprised between 116 and 119°. Thus, when going from a pure Sn to a pure Ga layer, the mean angle $\bar{\alpha}$ varies from 101 to 117° reflecting a consequent flattening. Focusing now to models having the experimental D3 geometry, almost no change is observed in the lattice dimensions for optimized $Ca_4Ga_5Sn_3$ with respect to $Ca_4Ga_4Sn_4$. Instead a great increase of nearly 1 Å along the c-axis in $Ca_4Ga_3Sn_5$is caused by Sn enrichment. At the same time, the calculated formation enthalpy is slightly higher for substituted than for original $Ca_4Ga_4Sn_4$ models marking a destabilization. But with an increase by only 0.02eV per atom, $Ca_4Ga_5Sn_3$ appears just very little less stable than $Ca_4Ga_4Sn_4$ whereas formation of $Ca_4Ga_3Sn_5$ is two times more destabilizing. The experimental angle of 112.13° measured in $Ca_4Ga_{4+x}Sn_{4-x}$ at composition $Ca_4Ga_{4.9}Sn_{3.1}$ is larger than mean value of 109° for Ga–

Sn layers and it lies on the scale of angles between values for Ga–Sn and Ga–Ga layers, in quite good agreement with the actual composition Ga–$Sn_{0.8}Ga_{0.2}$ of the layer. Contrary to what occurs for $Ca_4Ga_4Sn_4$ composition, the distance of 3.276 Å between layers in optimized $Ca_4Ga_5Sn_3$ properly fits the experimental distance of 3.222 Å in $Ca_4Ga_{4.9}Sn_{3.1}$.

4.7. Structural accommodation of $Ca_4Ga_{4+x}Sn_{4-x}$

According to the present and the previous structural studies, $Ca_4Ga_{4+x}Sn_{4-x}$ is found to exist at least for x = 0 and x ~ 1, with similar lattices and geometries. The question is how the structure can accommodate the composition and then the electron-content variations. A simple picture of the bonding is provided by a rigid band model calculation for the experimental arrangement in which Sn totally fills the M1 site and Ca is considered only as a potential electron donor.

The band structure computed for this network (figure 7) displays a small direct gap for an electron content of 36 that corresponds to the composition $Ca_4Ga_4Sn_4$. A look at the crystal orbital overlap populations is more informative indicating the nature of interactions in a specific energy range. The overall interactions are bonding up to 35.6 and clearly antibonding above 36 electrons, then filling the bands up to 36 electrons ($Ca_4Ga_4Sn_4$) leads to an optimal situation in terms of bonding. Nevertheless, the total overlap population has an extremely weak negative value between 35.6 and 36 and is naught for 35.6 electrons. An equilibrium is then reached also for an electron content of 36.5 which precisely corresponds to the composition $Ca_4Ga_{4.5}Sn_{3.5}$ determined from analysis of our single crystal. Within the energy range from 35.6 to 36 electron-filling, the bands mainly result from p_z atomic orbitals contributions and display rather nonbonding character. These bands are able to accommodate the electron content variations and are greatly involved in puckering of the hexagon layers. The Sn–Ga interactions within layers display a weak antibonding character between 34.5 and 36 electrons while Ga–Ga interactions between the layers are bonding all over

the energy range with a maximum overlap population just above 35 electrons. Note that with 37 electrons the Sn-rich composition $Ca_4Ga_3Sn_5$ would display clearly antibonding overall interactions.

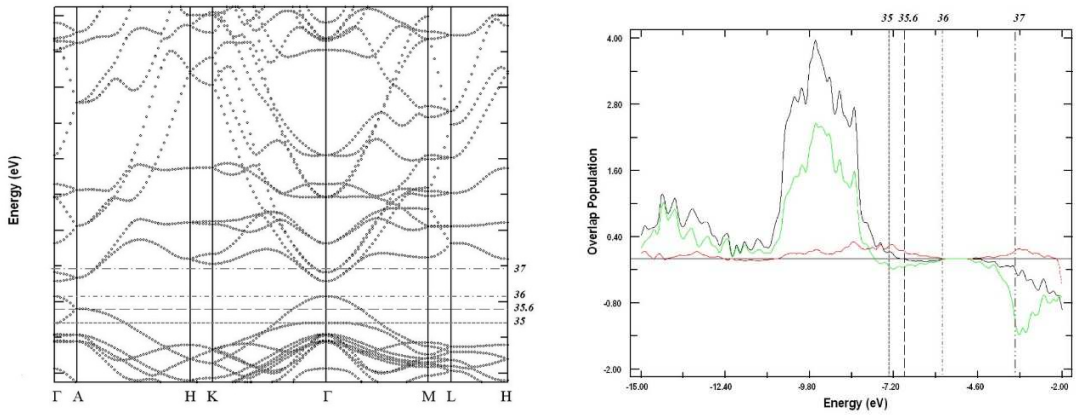

Figure 7: *left* –density of states calculated within a rigid model; *right* –crystal orbital overlap populations for all bonds (black), Sn–Ga intra-layer bonds (green) and Ga–Ga interlayer bonds (red). Fermi level is represented for filling with 35, 35.6, 36 and 37 electrons.

Actually, CASTEP band structures calculated at the DFT level for $Ca_4Ga_4Sn_4$ and $Ca_4Ga_5Sn_3$ are globally similar and characteristic of a metallic behavior (see in supplementary material). No band crosses the Fermi level at the HK segment of the irreducible Brillouin zone (also at ML segment for $Ca_4Ga_5Sn_3$), thus compound $Ca_4Ga_{4+x}Sn_{4-x}$ is expected to display some anisotropy in its electrical conduction.

5. Conclusion

The structure of compounds $SmGaSn_2$ and $Ca_4Ga_{4.9}Sn_{3.1}$ has been solved and refined from X-ray single crystal data. Cubic $SmGaSn_2$ is characterized with Sn/Ga atomic mixing at all positions and

may be seen as derived from $SmSn_3$ by atomic substitution. Moreover, analogies in their band structures allows to expect intermetallic heavy fermion properties for $SmGaSn_2$. Hexagonal $Ca_4Ga_{4.9}Sn_{3.1}$ is isostructural with $Ca_4Ga_4Sn_4$ and also displays atomic mixing. The significant differences noted in their geometries are most probably due to a poor quality of the powder data structure determination of $Ca_4Ga_4Sn_4$ [6]. The information collected in this work particularly from DFT calculations tends to prove the existence of a composition domain for $Ca_4Ga_{4+x}Sn_{4-x}$ in the range $0 \leq x \leq 1$, excluding a possible extension on the Sn-rich side. It should also be stressed that partial atomic ordering occurs within the (Sn,Ga) sub-lattice in $Ca_4Ga_{4+x}Sn_{4-x}$ as also described in a ternary intermetallic compound with samarium [45].

References

[1] S. Okada, K. Kudou, T. Shishido, I. Higashi, H. Horiuchi, T. Fukuda,
J. Alloys compd., 281 (2) (1998), pp. 160-162.

[2] T. Shishido, M. Oku, S. Okada, K. Kudou, J. Ye, T. Sasaki, Y. Watanabe, N. Toyota, H. Horiuchi, T. Fukuda,
J. Alloys Compd., 281 (2) (1998), pp. 196-201.

[3] S. Ukei, T. Shishido, T. Fukuda,
Acta Crystallogr., C 45 (1989), pp. 349-350.

[4] S. Ukei, T. Shishido, T. Fukuda,
Acta Crystallogr., C 46 (1990), pp. 1193-1195.

[5] S. Ukei, T. Shishido, T. Fukuda,
Acta Crystallogr., C 46 (1990), pp. 1195-1197.

[6] A. Czybulka, B. Pinger, H. U. Schuster,
Z. Anorg. Allg. Chem., 579 (1989), pp. 151-157.

[7] J. Stöhr, H. Schäfer,
Z. Anorg. Allg. Chem., 474 (1981), pp. 221-225.

[8] C. Blase, G. Cordier,
Z. Naturforsch., B44 (1989), pp. 1479-1482.

[9] C. Blase, G. Cordier,
Z. Naturforsch., 44B (1989), pp. 1011-1014.

[10] W. Müller, J. Stöhr,
Z. Naturforsch., B32 (1977), pp. 631-636.

[11] G. M. Sheldrick,
SHELXS 97. A Program for Crystal Structures Solution. University of Göttingen. Germany, (1997).

[12] G. M. Sheldrick,
SHELXL97: A Program for Refining Crystal Structures. University of Göttingen. Germany, (1997).

[13] G. Kresse, J. Furthmuller,
J. Comput. Mater. Sci., 6 (1996), pp. 15-50.

[14] J. P. Perdew, J. A. Chevary, S. H. Vosko, M. R. Pederson, D. J. Singh, C. Fiolhais,
Phys. Rev. B, 46 (1992), pp. 6671-6687.

[15] D. Vanderbilt,
Phys. Rev. B, 41 (1990), pp. 7892-7895.

[16] H. J. Monkhorst, J. D. Pack,
Phys. Rev. B, 16 (1997), pp. 1748-1749.

[17] J. Ren, W. Liang, M. H. Wangbo,
CAESAR2 Package for Windows. Crystal And Electronic Structure AnalyseR , North Carolina State University, (2002).

[18] M. Wendorff, C. Röhr,
Z. Anorg. Allg. Chem., 637 (2011), pp. 1013-1023.

[19] T. Charvolin, A. Blaise, M. N. Bouillet, P. Burlet, J. M. Fournier, J. Larroque, J. M. Rossat Mignod, J. P. Sanchez,
J. Magn. Magn. Mater., 132 (1994), pp. 46-54.

[20] M. Tillard, D. Zitoun, C. Belin,
Inorg. Chem., 48 (2009), pp. 2399-2406.

[21] Y. N. Grin, A. O. Fedorchuck,
Russ. Metall., 5 (1992), pp. 197-200.

[22] M. J. Evans, Y. Wu, V. F. Kranak, N. Newman, A. Reller, F. J. Garcia Garcia, U. Häussermann,
Phys. Rev. B, 80 (064514) (2009), pp. 1-11.

[23] E. J. Felten,
J. Am. Chem. Soc., 78 (1956), pp. 5977-5978.

[24] M. E. Jones, R. E. Marsh,
J. Am. Chem. Soc., 76 (1954), pp. 1434-1436
[25] H. Axel, K. H. Janzon, H. Schäfer, A. Weiss,
Z. Naturforsch., B23 (1968), pp. 108-109.

[26] S. Kuroiwa, T. Kakiuchi, H. Sagayama, H. Sawa, J. Akimitsu,
Physica C, 460/462 (2007), pp. 154-155
[27] B. Eisenmann, M. Rhode, M. Wendorff, C. Röhr,
Z. Anorg. Allg. Chem., 634 (2008), pp. 153-165.

[28] J. W. Nielsen, N. C. Baenziger,
Acta Crystallogr. , 7 (1954), pp. 132-133.

[29] M. Wörle, R. Nesper, G. Mair, M. R. Schwarz, H. G. Von Schnering,
Z. Anorg. Allg. Chem., 621 (1995), pp. 1153-1159.

[30] I. I. Mazin, D. A. Papaconstantopoulos,
Phys. Rev. B, 69 (18) (2004), pp. 180512.

[31] E. I. Gladyshevskii,
Dopov. Akad. Nauk Ukr. RSR (1964), pp. 209-212.

[32] A. Iandelli,
Z. Anorg. Allg. Chem., 330 (1964), pp. 221-232.

[33] R. D. Hoffmann, R. Pöttgen,
Z. Kristallogr. , 216 (3) (2001), pp. 127-145.

[34] P. Manfrinetti, M. Pani,
J. Alloys Compd., 393 (1–2) (2005), pp. 180-184.

[35] V. Pavlyuk, I. Oshchapovsky, B. Marciniak,
J. Alloys Compd., 477 (1–2) (2009), pp. 145-148.

[36] Y. Janssen, S. Chang, B. K. Cho, A. Llobet, K. W. Dennis, R. W. McCallum, R. J. McQueeney, P. C. Canfield,
J. Alloys Compd., 389 (1–2) (2005), pp. 10-13.

[37] J. R. Salvador, F. Guo, T. Hogan, M. G. Kanatzidis,
Nature, 425 (6959) (2003), pp. 702-705.

[38] T.-S. You, Y. Grin, G. J. Miller,
Inorg. Chem., 46 (21) (2007), pp. 8801-8811.

[39] T.-S. You, J.-T. Zhao, R. Pöttgen, W. Schnelle, U. Burkhardt, Y. Grin, G. J. Miller, J. Solid State Chem., 182 (9) (2009), pp. 2430-2442.

[40] C. Blase, G. Cordier, R. Kniep, Z. Anorg. Allg. Chem., 619 (1993), pp. 1161-1166.

[41] R. D. Shannon, Acta Crystallogr. A, 32 (1976), pp. 751-767.

[42] M. J. Evans, G. P. Holland, F. J. Garcia Garcia, U. Häussermann, J. Am. Chem. Soc., 130 (2008), pp. 12139-12147.

[43] W. Harms, M. Wendorff, C. Röhr, Z. Naturforsch., B62 (2007), pp. 177-194.

[44] G. Wenski, A. Mewis, Z. Kristallogr., 176 (1986), pp. 125-134

[45] Y. O. Tokaychuk, Y. E. Filinchuk, A. O. Fedorchuk, O. I. Bodak, Acta Crystallogr., C59 (2003), pp. i125-i127.